Biosensors and Bioelectronics 57 (2014) 149–156

Contents lists available at ScienceDirect

Biosensors and Bioelectronics

journal homepage: www.elsevier.com/locate/bios

Polyoxometalate@magnetic graphene as versatile immobilization matrix of $Ru(bpy)_3^{2+}$ for sensitive magneto-controlled electrochemiluminescence sensor and its application in biosensing

Jing Qian, Kun Wang*, Yicong Jin, Xingwang Yang, Ling Jiang, Yuting Yan, Xiaoya Dong, Huaming Li, Baijing Qiu

Key Laboratory of Modern Agriculture Equipment and Technology, School of Chemistry and Chemical Engineering, Jiangsu University, Zhenjiang 212013, PR China

ARTICLE INFO

Article history:
Received 4 December 2013
Received in revised form
28 January 2014
Accepted 5 February 2014
Available online 13 February 2014

Keywords:
Magnetic graphene
Polyoxometalate
$Ru(bpy)_3^{2+}$
Electrochemiluminescence
NADH
L-Lactate

ABSTRACT

We demonstrated here the exploration of polyoxometalate (POM) coated magnetic Fe_3O_4/reduced graphene oxide (POM@mrGO) composite as the versatile immobilization matrix for the electrochemiluminescence (ECL) agent $Ru(bpy)_3^{2+}$. The effective modification of $Ru(bpy)_3^{2+}$/POM@mrGO hybrid simply involved using magnetic electrode showed 10-fold ECL intensity increase than that observed for $Ru(bpy)_3^{2+}$/Nafion@mrGO to the same concentration of nicotinamide adenine dinucleotide (NADH), which is largely due to POM's good electrocatalytic activity towards NADH oxidation. These findings allowed the stable and ultrasensitive ECL detection of NADH as low as 0.1 nM. The good stability and high sensitivity of the magneto-controlled ECL sensor enabled us to explore the feasibility of applying the sensing platform to fabricating the ECL biosensors in which the NADH was produced from the dehydrogenase-based enzymatic reaction in the presence of NAD^+ cofactor. With L-lactate dehydrogenase as a model, a L-lactate biosensor was successfully constructed where we showed that the ECL intensity of the biosensor increased with the increasing L-lactate concentration. Excellent performance of the presented biosensor has been achieved including a wide linear range extended from 5.0×10^{-9} M to 5.0×10^{-4} M and an extremely low detection limit of 0.4 nM. Such sensing strategy combines enzymatic selectivity with simple sensor preparation can be used as a new and biocompatible platform for dehydrogenase-based ECL biosensing.

1. Introduction

Nowadays, Ruthenium (II) tris(bipyridine) ($Ru(bpy)_3^{2+}$)-based electrochemiluminescence (ECL) sensors have been one of the main focuses in the ECL field due to its great scientific and technological importance to clinical analysis and biomolecule detection (Lin et al., 2009; Bertoncello and Forster, 2009; Zhan and Bard, 2007). It is believed that the immobilization of $Ru(bpy)_3^{2+}$ on a solid support can provide significant advances compared with the solution-phase $Ru(bpy)_3^{2+}$ ECL system, such as reducing the consumption of expensive reagents and simplifying the experimental design (Cao et al., 2013; Li et al., 2011). Generally, a lot of efforts have been devoted to finding new and effective strategies for the immobilization of $Ru(bpy)_3^{2+}$ on a solid electrode surface by embedding $Ru(bpy)_3^{2+}$ in ion-exchangeable polymer film (Zhang et al., 2006), in sol–gels (Deng et al., 2009), and self-assembling monolayer (Sun et al., 2005), or by the Langmuir–Blodgett technique (Moretto et al., 2010). However, these ECL sensors are either expensive or complexed, and even in most cases, the ECL responses are still subject to low stability and sensitivity (Gao et al., 2007). From this regard, searching for a solid-state ECL sensor with simplicity and speed as well as high sensitivity and long-term stability has stimulated the development of more efficient matrix for the immobilization of $Ru(bpy)_3^{2+}$.

Recently, quite a few nanomaterials, such as silica nanoparticles (Yang et al., 2010), carbon nanotubes (CNTs) (Mao et al., 2010a), and metal (Liu et al., 2009) or metal oxide (Mao et al., 2010b; Kim et al., 2005) nanoparticles have been used for the fabrication of the solid-state $Ru(bpy)_3^{2+}$ ECL sensors. Among all the known immobilization matrices, magnetic Fe_3O_4 nanoparticles have been brought into sharp focus largely due to their low toxicity, biocompatibility, and magnetic separation and modification which simply involves using external magnetic fields (Kim et al., 2005; Liao et al., 2013). Interestingly, the combination of magnetic nanoparticles and ECL

* Corresponding author.: Tel.: +86 511 88791800; fax: +86 511 88791708.
E-mail address: wangkun@ujs.edu.cn (K. Wang).

http://dx.doi.org/10.1016/j.bios.2014.02.005
0956-5663

reagents into one system are possible to simultaneously exhibit their respective properties and fulfill their potential use in multi-tasking applications, like e.g., ECL sensing and magnetic manipulation. However, several unavoidable problems are associated with pristine Fe_3O_4 nanoparticles, such as the possibility of self-agglomeration thus resulting in the loss of magnetism and dispersibility, as well as the ease with which they are oxidized when exposed to the atmosphere (Li et al., 2008). To overcome these difficulties, a relatively simple immobilization method based on ion-exchange of $Ru(bpy)_3^{2+}$ in Nafion-stabilized Fe_3O_4 nanoparticles has been demonstrated to be an efficient immobilization matrix to increase the sensitivity and stability of the magneto-controlled ECL sensor (Kim et al., 2005). More recently, Dong's group have developed a novel bifunctional nanoarchitecture by combing the magnetic Fe_3O_4 and luminescent $Ru(bpy)_3^{2+}$ encapsulated in silica nanoparticles (Zhang et al., 2007). With the protective layer of silica, a stable magneto-controlled ECL sensor was successfully constructed and further applied to detect tripropylamine and polyamines. Though some progress has been made in this field, new and efficient magnetic immobilization matrix are still needed to develop more robust, sensitive and stable ones.

Graphene, ever since its discovery in 2004, has evoked intensive attention due to its high carrier mobility, large specific surface area and outstanding electric conductivity (Liang et al., 2011; Jahan et al., 2012). With these amazing merits, graphene has been served as an ideal support for a number of inorganic nanoparticles such as gold nanoparticles (Hu et al., 2011), CdS nanocrystals (Wang et al., 2011), Ag_3PO_4 nanospheres (Ao et al., 2013), and Fe_3O_4 nanoparticles (Su et al., 2011; He and Gao, 2010; Chandra et al., 2010). Besides the attractive magnetic properties of Fe_3O_4/graphene composites, recent advances have also demonstrated that the combination of magnetic Fe_3O_4 nanoparticles with graphene sheets could efficiently avoid or decrease the self-aggregation possibility of Fe_3O_4 particles and the stacking of individual graphene sheets (He and Gao, 2010; Chandra et al., 2010). These results consequently provide some distinguished properties such as a larger surface area and a higher adsorption capacity for the incorporated molecules. In a recent study, $Ru(bpy)_3^{2+}$ solution was dripped on the Nafion-functionalized magnetite/graphene composites modified screen-printed electrode to obtain a solid-state ECL sensor (Xu et al., 2013). With tripropylamine as the co-reactant, the prepared ECL sensor displayed a better stability and 2.5-fold signal enhancement when the external magnet was applied. As polyoxometalates (POMs) are proved to be suitable inorganic building blocks for the construction of functional thin films with negatively charged surface, POM-functionalized Fe_3O_4/graphene might act as an optimum alternative to immobilize $Ru(bpy)_3^{2+}$. Besides, functional films containing POMs can catalyze the reduction of XO^{3-} (X=Cl, Br, I) and the oxidation of $C_2O_4^{-}$, adrenaline, and nicotinamide adenine dinucleotide (NADH) (Li et al., 2012). As NADH controls the enzymatic activity of more than 300 dehydrogenases, the functional films containing POMs have promising applications in fabricating dehydrogenases-based biosensors to determine a number of clinically important analytes such as lactates, alcohols, and aldehydes.

Here we report the synthesis of POM coated Fe_3O_4/reduced graphene oxide (POM@mrGO) composites and demonstrated their use as versatile immobilization matrix of $Ru(bpy)_3^{2+}$ for the first time. The POM functional film on mrGO surface served as not only the protective layer of Fe_3O_4 particles but also the anchoring sites with multiple anionic moiety, to which $Ru(bpy)_3^{2+}$ cations were immobilized via a simple self-assembly strategy. Due to the excellent electrocatalytic activity of POM toward NADH oxidation, we explored the feasibility of applying them to fabricating a magneto-controlled ECL sensor for NADH detection with large response. On the basis of these findings, a model enzyme L-lactate dehydrogenase (LDH) was then immobilized on the solid film to expand its application in dehydrogenase-based biosensors.

2. Experimental

2.1. Materials and chemicals

$Ru(bpy)_3Cl_2 \cdot 6H_2O$, NADH (disodium salt, trihydrate), NAD^+, LDH (from bovine heart, 513 units mg^{-1}), Nafion (5 wt%), and L-lactate were purchased from Sigma-Aldrich. Ferric chloride ($FeCl_3$), sodium acetate (NaAc), ethylene glycol (EG), and $H_3PMo_{12}O_{40}$ were purchased from Sinopharm Chemical Reagent Co., Ltd. mrGO composites were synthesized with our reported one-step solvothermal method (Jin et al., 2013) described in the Supporting information. All the reagents were of analytical grade and used as received. Double-distilled water was used throughout the study.

2.2. Apparatus

The morphology and size of the samples were analyzed with scanning electron microscope (SEM, JEOL JSM-6700, Japan). X-ray photoelectron spectroscopy (XPS) was performed on ESCALAB 250 multitechnique surface analysis system (Thermo Electron Co., USA). The software named XPS Peak (version 4.1) has been used in the deconvolution process of XPS spectrum. Magnetic measurements were carried out using a BHV-55 Vibrating sample magnetometer. Photoluminescence (PL) spectra were recorded using a Cary Eclipse fluorescence spectrophotometer (Varian Co., Ltd., U.S.A.). Cyclic voltammograms (CVs) and ECL measurements were monitored by a MPI-A multifunctional chemiluminescent analytical system (Xi'an Remex Analyze Instrument Co., Ltd., China) with the voltage of the photomultiplier tube set at 800 V. All the electrochemical experiments were carried out in a conventional three-electrode system comprised of a platinum wire auxiliary, a saturated Ag/AgCl reference, and the magnetic glassy carbon electrode (mGCE, 10 mm in diameter and 65 mm in length) with an inserted glassy carbon (3 mm in diameter and 2 mm in depth) working electrode. The mGCE was purchased from Tianjin Incole Union Technology Co., Ltd. (Tianjin China).

2.3. Preparation of $Ru(bpy)_3^{2+}$/POM@mrGO hybrid

5 mg of $H_3PMo_{12}O_{40}$ was firstly dissolved in 5 mL water and then the pH of the solution was adjusted to 4.5 by using 1.0 M NaOH under stirring. Afterwards, 25 mg of mrGO composites was added into the above solution and the mixture was stirred for 1 h at room temperature. POM@mrGO was thus obtained with magnetic separation and then redispersed in 5 mL water by hand-shaking. After that, 60 μL of 0.1 M $Ru(bpy)_3^{2+}$ aqueous solution was added into the above suspension and stirred for another 1 h, followed by magnetic separation and washing with water for several times. Finally, the required $Ru(bpy)_3^{2+}$/POM@mrGO hybrid was dried for later use. For comparison, $Ru(bpy)_3^{2+}$/Nafion@mrGO hybrid was also synthesized following the discription in Supporting information.

2.4. Sensor construction

Prior to each modification, the mGCE was first polished with polishing clothes and 1.0, 0.3, and 0.05 μm alumina slurry. After successive sonication in ethanol and water, the electrode was rinsed with water and allowed to dry at room temperature. 8 mg of the as-prepared $Ru(bpy)_3^{2+}$/POM@mrGO or $Ru(bpy)_3^{2+}$/Nafion@mrGO hybrid was dispersed in 200 mL water. After that, the pretreated mGCE was immersed shallowly in 3 mL of the above suspension,

nearly all the hybrid was assembled on the electrode surface in 3 min by magnetism without any fixing agent. $Ru(bpy)_3^{2+}$/POM@mrGO hybrid modified mGCE ($Ru(bpy)_3^{2+}$/POM@mrGO–mGCE) or $Ru(bpy)_3^{2+}$/Nafion@mrGO hybrid modified mGCE ($Ru(bpy)_3^{2+}$/Nafion@mrGO–mGCE) was thus successfully constructed. LDH was immobilized on the surface of $Ru(bpy)_3^{2+}$/POM@mrGO–mGCE by a simple casting method to construct a biosensor. Brifely, 0.2 mg of LDH was dispersed in 1 mL 0.1 M pH 7.4 PBS. 6 μL of the proposed solution was cast onto the surface of $Ru(bpy)_3^{2+}$/POM@mrGO–mGCE, which was dried in air at room temperature to form LDH-$Ru(bpy)_3^{2+}$/POM@mrGO–mGCE.

3. Results and discussion

3.1. Morphology and composition characterization

SEM image of mrGO composites suggested that the Fe_3O_4 nanospheres with a diameter range of 100–260 nm and rough surface were densely and randomly planted on the rGO sheet, where an individual Fe_3O_4 nanosphere was constructed with some smaller nanoparticles (Fig. 1A). Such rough structure of Fe_3O_4 nanospheres could provide a large surface area to facilitate the rapid mass diffusion and POM coating. After treated with $H_3PMo_{12}O_{40}$, one of the most typical POMs, an additional film was found to be coated on the mrGO surface, suggesting the successful formation of POM@mrGO hybrid as shown in Fig. 1B. This POM functional film could perform dual roles: the protective layer of Fe_3O_4 nanospheres to prevent the oxidation as well as the anchoring sites to bond multiple cationic species such as $Ru(bpy)_3^{2+}$ due to the abundant anionic moieties on the surface. The morphology of $Ru(bpy)_3^{2+}$/POM@mrGO hybrid was much similar to that of the POM@mrGO hybrid (Fig. 1C) and the rough surface gave superiority in potential application of enzyme loading. The chemical composition of $Ru(bpy)_3^{2+}$/POM@mrGO hybrid was ascertained by XPS analysis, as shown in Fig. 2. The peaks of Fe, O, P, Mo, N, C, and Ru elements were successfully achieved, demonstrating the constituent elements of the as-prepared hybrid in accordance with mrGO, $[PMo_{12}O_{40}]^{3-}$, and $Ru(bpy)_3^{2+}$. Considering the negative charge of $[PMo_{12}O_{40}]^{3-}$ and the postive charge of $Ru(bpy)_3^{2+}$, electrostatic attractions between them may impulse the formation of $Ru(bpy)_3^{2+}$/POM@mrGO hybrids.

3.2. Magnetic property analysis

Magnetization curves, as shown in Fig. 3A, were measured on powder samples of mrGO (curve a) and $Ru(bpy)_3^{2+}$/POM@mrGO (curve b) at 298 K. Both samples exhibited a nonlinear and reversible behavior with an almost immeasurable magnetic hysteresis loop and negligible remanence effect, typical of a superparamagnetic character. The saturation magnetization of mrGO and $Ru(bpy)_3^{2+}$/POM@mrGO was 83 and 70 emu g^{-1}, respectively. The strong magnetization (>40 emu g^{-1}) of both samples benefitted form the high content of Fe_3O_4 particles planted on the graphene sheets. Compared with mrGO, the relatively low saturation magnetization of $Ru(bpy)_3^{2+}$/POM@mrGO could be attributed to the successful attachment of the nonmagnetic $Ru(bpy)_3^{2+}$ and POM on mrGO. As demonstrated as inset of Fig. 3A, $Ru(bpy)_3^{2+}$/POM@mrGO hybrid could be directed to specific locations when manipulated by an external magnetic field, this advantage was in favor of the magnetic field-driven separation and the magneto-controlled modification onto electrode surface under an external magnetic field.

3.3. Emission properties study

The emission spectrum of the as-prepared $Ru(bpy)_3^{2+}$/POM@mrGO hybrid was compared with that of the POM@mrGO and $Ru(bpy)_3^{2+}$ aqueous solution (Fig. 3B). The maximum emission peak of free $Ru(bpy)_3^{2+}$ (curve a) was observed at about 610 nm which resulted from the triple metal-to-ligand charge-transfer state (Qian and Yang, 2007). On the contrary, the POM@mrGO (curve b) was found to be nonemissive upon light excitation. Judging from curve c in Fig. 3B, the $Ru(bpy)_3^{2+}$/POM@mrGO hybrid gave rise to a similar emission peak at about 613 nm originating from the characteristic emission of $Ru(bpy)_3^{2+}$ (Qian et al., 2010). Compared to the free $Ru(bpy)_3^{2+}$, the slight red shift phenomenon for emission peak was further proving the strong electrostatic interaction between $Ru(bpy)_3^{2+}$ and $[PMo_{12}O_{40}]^{3-}$. All the results indicated that $Ru(bpy)_3^{2+}$ was successfully incorporated which could uphold its luminescence properties well.

3.4. Electrochemistry and ECL investigation

A magnetic electrode was used to accumulate $Ru(bpy)_3^{2+}$/POM@mrGO hybrid onto the electrode surface, which made the modification process simple, effective and reversible. CVs of $Ru(bpy)_3^{2+}$/POM@mrGO–GCE in 0.1 M PBS (pH 7.4) at different scan rates were shown in Fig. 4A. There was a couple of redox peaks in the potential range from 0.5 to 1.2 V, which was attributed to the one-electron redox reaction of $Ru(bpy)_3^{2+}$ (Sun et al., 2007; Wang et al., 2010). It was found that the anodic peak current was proportional to the square root of scan rate ($\upsilon^{1/2}$) over the range of 20–500 mV s^{-1} (inset of Fig. 4A), indicating that the immobilized $Ru(bpy)_3^{2+}$ contained in the hybrids on the electrode surface underwent a diffusion-controlled process within the film (Du et al., 2005; Zhang et al., 2007). Moreover, the difference between the anodic and cathodic peak potentials (ΔE_p) was 150 mV at the scan rate of 100 mV s^{-1} and the ΔE_p values became larger with the increasing scan rate. These behaviors could be attributed to the hysteresis of the Ru(III)/Ru(II) reactions in the adsorbed layer at higher scan rates, showing that this electrochemical process was quasi-reversible under the present conditions (Wu et al. 2013; Li et al. 2012).

Fig. 4B showed CVs and corresponding ECL intensity–potential curves (inset) of the $Ru(bpy)_3^{2+}$/POM@mrGO–mGCE in the absence (curve a) and presence (curve b) of 0.2 mM NADH at a scan rate of 100 mV s^{-1} in 0.1 M pH 7.4 PBS. A pair of redox waves of Ru

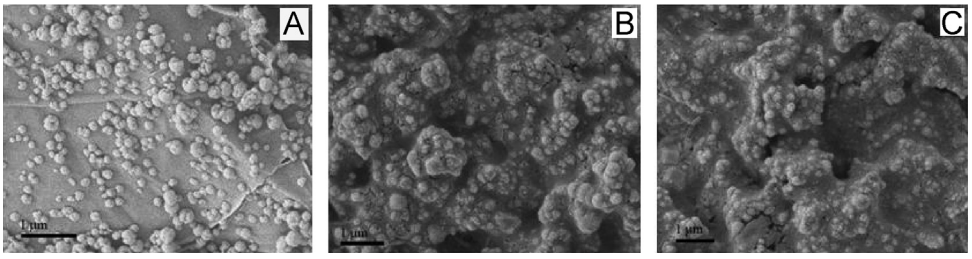

Fig. 1. SEM images of the as-prepared mrGO (A), POM@mrGO (B), and $Ru(bpy)_3^{2+}$/POM@mrGO hybrids (C).

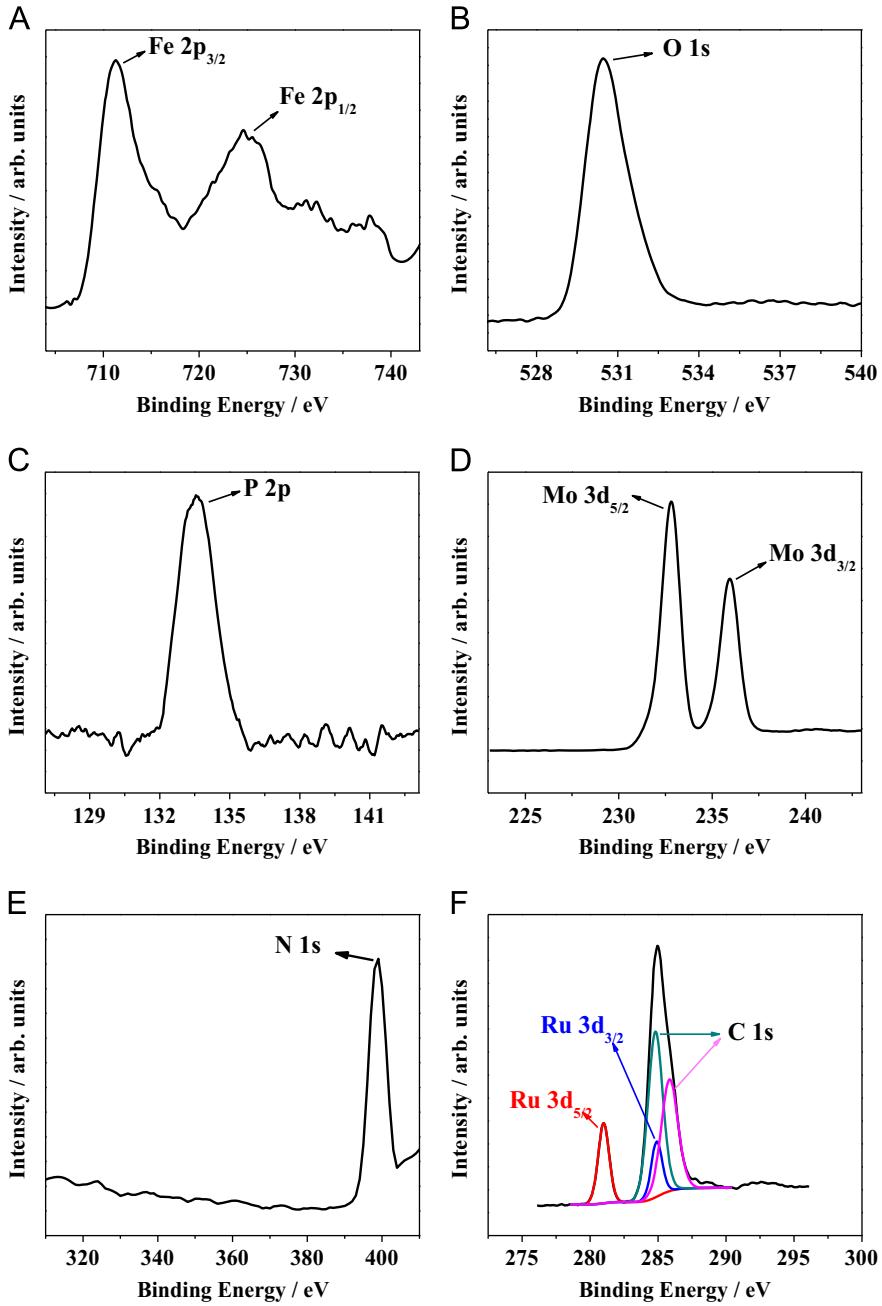

Fig. 2. XPS spectra of Fe 2p (A), O 1s (B), P 2p (C), Mo 3d (D), N 1s (E), and C 1s and Ru 3d (F) obtained from $Ru(bpy)_3^{2+}$/POM@mrGO hybrids.

$(bpy)_3^{2+}$ existed and a very low ECL emission (816 a.u.) was observed with the absence of NADH. After adding 0.2 mM NADH into the electrolyte solution, in parallel, the oxidative peak current of $Ru(bpy)_3^{2+}$ significantly increased with the reductive current decreased. About 1.7-fold peak current enhancement was obtained owing to the presence of NADH. Accordingly, the ECL signal increased considerably once the NADH was added and a strong ECL signal with intensity as high as 9300 a.u. was given at the NADH concentration of 0.2 mM (inset of Fig. 4B). In the presence of the NADH, the ECL mechanisms of $Ru(bpy)_3^{2+}$/POM@mrGO could be described by the following reaction scheme where an oxidative–reductive sequence occurred (Chovin et al., 2006; Milutinovic et al., 2011; Li et al., 2012):

$$NADH \rightarrow NADH^{\bullet +} + e^- \quad (1)$$

$$Ru(bpy)_3^{2+}/POM@mrGO \rightarrow Ru(bpy)_3^{3+}/POM@mrGO + e^- \quad (2)$$

$$Ru(bpy)_3^{3+}/POM@mrGO + NADH \rightarrow Ru(bpy)_3^{2+}/POM@mrGO + NADH^{\bullet +} \quad (3)$$

$$NADH^{\bullet +} \rightarrow NAD^{\bullet} + H^+ \quad (4)$$

$$Ru(bpy)_3^{3+}/POM@mrGO + NAD^{\bullet} \rightarrow Ru(bpy)_3^{2+*}/POM@mrGO + NAD^+ \quad (5)$$

$$Ru(bpy)_3^{2+*}/POM@mrGO \rightarrow Ru(bpy)_3^{2+}/POM@mrGO + h\nu_{ECL} \quad (6)$$

More specifically, NADH and the immobilized $Ru(bpy)_3^{2+}$ could be electrochemically oxidized on the electrode surface at their respective potentials (reactions (1) and (2)). Meanwhile, NADH could also be oxidized homogeneously by $Ru(bpy)_3^{3+}$ (reaction (3)). The radical cation $NADH^{\bullet +}$ was deprotonated to form a highly reducing species $NAD^{\bullet}$ (reaction 4). In the next step, $NAD^{\bullet}$

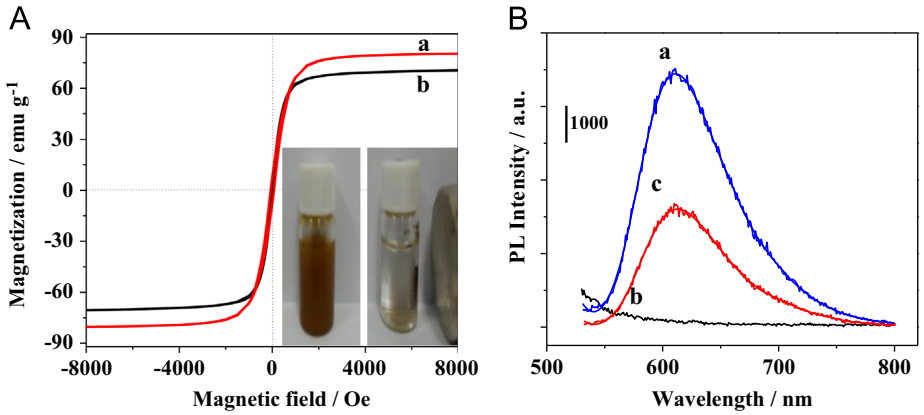

Fig. 3. (A) Magnetic hysteresis curves of mrGO (a) and $Ru(bpy)_3^{2+}$/POM@mrGO hybrid (b). Inset: photographic images of $Ru(bpy)_3^{2+}$/POM@mrGO suspension in the absence (left) and presence (right) of an external magnetic field. (B) PL spectra of free $Ru(bpy)_3^{2+}$ (a), POM@mrGO (b), and $Ru(bpy)_3^{2+}$/POM@mrGO (c) aqueous solution (excitation at 460 nm).

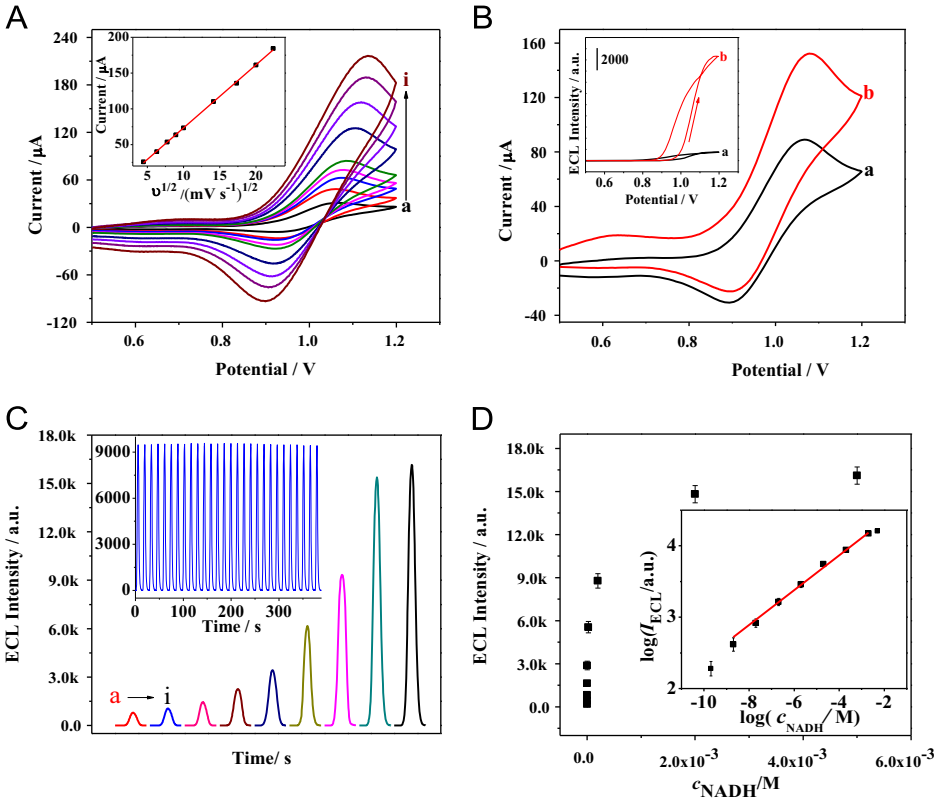

Fig. 4. (A) CVs of the ECL sensor at various scan rates (From a to i: 20, 40, 60, 80, 100, 200, 300, 400, and 500 mV s^{-1}) in 0.1 M pH 7.4 PBS. Inset: relationship between the anodic peak current and the $\upsilon^{1/2}$. (B) CVs of the ECL sensor in 0.1 M pH 7.4 PBS in the absence (a) and presence (b) of 0.2 mM NADH with a scan rate of 100 mV s^{-1}. Inset: the corresponding ECL responses. (C) Effect of NADH concentration on ECL intensity of the sensor in 0.1 M pH 7.4 PBS containing 2.0×10^{-10} (a), 2.0×10^{-9} (b), 2.0×10^{-8} (c), 2.0×10^{-7} (d), 2.0×10^{-6} (e), 2.0×10^{-5} (f), 2.0×10^{-4} (g), 2.0×10^{-3} (h), and 5.0×10^{-3} (i) M NADH. Inset: ECL emission of the ECL sensor in 0.1 M pH 7.4 PBS containing 0.2 mM NADH with continuous CVs. (D) Calibration curves for NADH detection ($n=5$).

was reacted with $Ru(bpy)_3^{3+}$/POM@mrGO to produce NAD^+ and the excited state $Ru(bpy)_3^{2+*}$/POM@mrGO (reaction (5)). This homogeneous electron transfer (reaction (5)) was exergonic enough to populate the $Ru(bpy)_3^{2+*}$/POM@mrGO, while the initial electron transfer from NADH to $Ru(bpy)_3^{3+}$/POM@mrGO could not (Fukuzumi et al., 2003). Eventually, the excited $Ru(bpy)_3^{2+*}$/POM@mrGO species came back to their ground state $Ru(bpy)_3^{2+}$/POM@mrGO by emitting a photon (reaction (6)) and the ECL intensity was then monitored simultaneously.

In order to identify the function of POM in the electrochemical and ECL processes of $Ru(bpy)_3^{2+}$/POM@mrGO, the CVs (Fig. S1A) and ECL intensity–potential curves (Fig. S1B) of $Ru(bpy)_3^{2+}$/Nafion@mrGO–mGCE were acquired in 0.1 M pH 7.4 PBS in the absence (curve a) and presence (curve b) of 0.2 mM NADH. Fig. S1A showed that the electrochemical behaviors of $Ru(bpy)_3^{2+}$/Nafion@mrGO–mGCE had no obvious difference with and without NADH. In addition, the ECL intensity of the $Ru(bpy)_3^{2+}$/POM@mrGO–mGCE (curve b in inset of Fig. 4B) was about 10-fold enhancement than that observed for Ru $(bpy)_3^{2+}$/Nafion@mrGO–mGCE (curve b in Fig. S1B) to the same concentration of NADH. The comparative study indicated that the Ru $(bpy)_3^{2+}$/POM@mrGO hybrid could exhibit good electrocatalytic activity towards NADH oxidation while $Ru(bpy)_3^{2+}$/Nafion@mrGO could

not, which might be attributed to the fact that the POM could decrease the potential barriers of Eq. (1) (Li et al., 2012). Additionally, the large surface structure of the POM@mrGO could also facilitate the diffusion of NADH into the film and result in the large electrochemical and ECL responses occurring on the electrode interface.

With NADH as the probe, we evaluated the sensitivity of the prepared magneto-controlled ECL sensor. From Fig. 4C, we could see that the ECL signal increased as the concentration of NADH in the tested solution increased. Calibration curve was plotted on logarithmic axes to show a very wide dynamic range from 2.0×10^{-9} to 2.0×10^{-3} M with a regression equation of the form $\log I_{ECL}=4.8411+0.2457\log(c_{NADH}/M)$ and the correlation coefficient $R^2=0.9942$, where I_{ECL} was the ECL intensity and c_{NADH} was the concentration of NADH (Fig. 4D). The detection limit was estimated to be 0.1 nM based on $S/N=3$, which was 10-fold lower than the ion-exchangeable sol–gel co-immobilized $Ru(bpy)_3^{2+}$-modified electrode (Deng et al., 2009), 200-fold lower than that of the multilayer films $(LDH/PSS/Ru(bpy)_3^{2+}/PSS)_n$ modified electrode (Choi et al., 2007), and 3000-fold lower than that of $Ru(bpy)_3^{2+}$/CNTs-titania-Nafion modified electrode (Zhang et al., 2012). The high sensitivity of the presented sensor could be ascribed to the following advantages: (1) POM@mrGO composites could immobilize a large amount of Ru $(bpy)_3^{2+}$ molecules on the basis of the considerable large surface area of mrGO; (2) the presence of POM functional film could exhibit excellent electrocatalytic ability to NADH oxidation and result in an ECL signal enhancement occurring at the electrode interface (Li et al., 2012). The stability of the ECL sensor was also studied. As shown in inset of Fig. 4C, nearly no ECL decrease was observed under continuous potential scanning for 28 cycles in 0.1 M pH 7.4 PBS containing 0.2 mM NADH and the relative standard deviation (RSD) was only 0.48%. The long-term stability of the ECL sensor was investigated during one month. The results suggested less than 8.3% decrease in ECL response to 0.2 mM NADH over this period. The surprising stability can be attributed to the long-term stability of Fe_3O_4 with the protective layer to prevent oxidation and the superiority of the magnetic field-driven electrode modification strategy.

3.5. Application in dehydrogenase-based ECL biosensor

The good stability and high sensitivity of the presented ECL sensor towards NADH enable us to explore the feasibility of applying the sensing platform to fabricating the ECL biosensors in which the NADH is produced from the dehydrogenase-based enzymatic reaction in the presence of NAD^+ cofactor. Using LDH as the model dehydrogenase, we demonstrated the use of Ru $(bpy)_3^{2+}$/POM@mrGO hybrid as an electronic transducer for the development of integrated ECL biosensor for L-lactate sensing. The reaction of L-lactate catalyzed by LDH was illustrated as follows (Zhang et al., 2012):

$$\text{L-lactate}+NAD^+ \overset{LDH}{\rightleftharpoons} \text{pyruvate}+NADH+H^+$$

From the corresponding relationship between the regenerated NADH and the consumed L-lactate according to the reaction mechanism, the increased ECL response of NADH was used to represent the increasing L-lactate concentration. Fig. 5A showed the ECL responses of LDH/$Ru(bpy)_3^{2+}$/POM@mrGO–mGCE in 0.1 M pH 7.4 PBS containing 5 mM NAD^+ at different concentrations of L-lactate. As indicated, the ECL intensity increased as the concentration of L-lactate in the tested solution increased. The standard calibration curve for L-lactate determination was shown in Fig. 5B. The ECL intensity increased in a linear fashion for the L-lactate concentration ranging from 5×10^{-9} M to 5×10^{-4} M with a detection limit of 0.4 nM at $S/N=3$. A linear equation of $\log I_{ECL}=4.9638+0.2354\log(c_{L\text{-lactate}}/M)$ was obtained with the correlation coefficient $R^2=0.9790$, where I_{ECL} was the ECL intensity and $c_{L\text{-lactate}}$ was the L-lactate concentration. The analytical performance of the proposal biosensor for L-lactate has been compared with other sensors reported in the literatures. Characteristics such as the linear range of the corresponding calibration graph, and the limit of detection achieved are all summarized in Table 1. As can be seen from Table 1, the proposal biosensor possessed a broader linear range and a very low detection limit. Its sensitivity was approximately 1000-fold higher than corresponding values observed in most of the electrochemical or chemiluminescent L-lactate biosensors, and even much higher than that of the luminol-based ECL method, the detection limit of which was down to 4 nM (Haghighi et al., 2011) or 2.4 μM (Martínez et al., 2009).

The selectivity of the biosensor was evaluated by the comparison of the sensing results of 40 μM of ascorbic acid (AA), 120 μM of glucose, and 40 μM of uric acid (UA). As shown in inset of Fig. 5A, the response signals to above three common interfering agents were negligible compared with the blank solution while an obvious increase in ECL response was observed for 0.5 mM L-lactate, attributing to the specific recognition force of LDH to L-lactate, which suggested the biosensor possessed high selectivity. A series of six successive measurements of 0.5 mM L-lactate on the same senor was found to yield a good reproducible signal with a RSD of 5.1%. The reproducibility of the biosensor was estimated by determining 0.5 mM L-lactate using six LDH/$Ru(bpy)_3^{2+}$/POM@mrGO–mGCEs

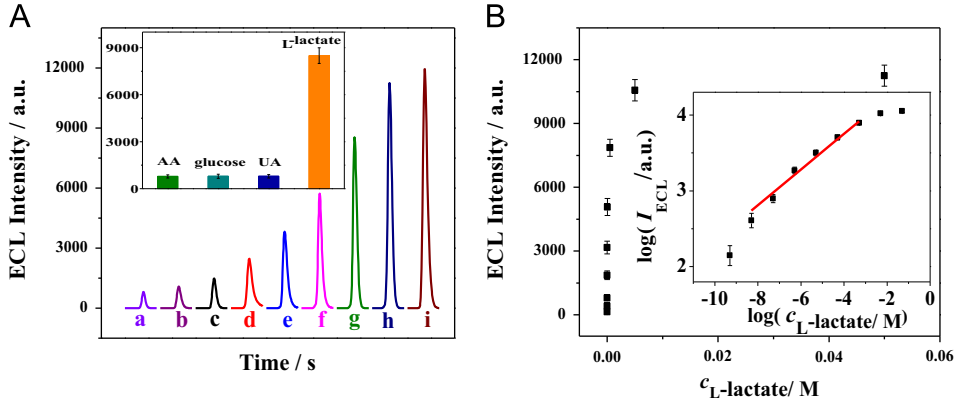

Fig. 5. (A) Effect of L-lactate concentration on ECL intensity of the biosensor in 0.1 M pH 7.4 PBS containing 5 mM NAD^+ and 5.0×10^{-10} (a), 5.0×10^{-9} (b), 5.0×10^{-8} (c), 5.0×10^{-7} (d), 5.0×10^{-6} (e), 5.0×10^{-5} (f), 5.0×10^{-4} (g), 5.0×10^{-3} (h), 5.0×10^{-2} (i) M L-lactate. Inset: selectivity of L-lactate biosensor ($n=5$). (B) Corresponding calibration curves for the detection of L-lactate ($n=5$).

Table 1
Characteristics of the present biosensor along with others reported in the literatures.

Sensor	Method	Linear range (μM)	Detection limit (μM)	Reference
nanoTiO_2/LDH–GCE	EC[c]	1–20	0.4	Cheng et al. (2008)
LDH–polysulfone/CNTs–SPCE[a]		1–20	0.37	Perez et al. (2012)
Nitrogen-doped CNTs/LOD[b]/Nafion–GCE		14–325	4.1	Goran et al. (2011)
LOD[b]/mesoporous silica/Nafion/CoPc–SPCE[a]		18.3–1500	18.3	Shimomura et al. (2012)
LDH/NAD^+/Fe_3O_4/CNTs–GCE		50–500	5	Teymourian et al. (2012)
luminol/LOD[b]/polyion complex membrane	CL[d]	50–4000	9.2	Ballesta-Claver et al. (2008)
LOD[b]/luminol–SPCE[a]	ECL	8–200	2.4	Martínez et al. (2009)
LOD[b]/nanoZnO/CNTs–GCE		0.01–10 and 10–200	0.004	Haghighi and Bozorgzadeh (2011)
LDH/$Ru(bpy)_3^{2+}$/POM@mrGO–mGCE		0.002–2000	0.0001	This work

[a] SPCE, screen-printed carbon electrode.
[b] LOD, lactate oxidase.
[c] EC, electrochemistry.
[d] CL, chemiluminescence.

prepared at the same condition. Six measurements from the batch resulted in a RSD of 9.1%, indicating acceptable reproducibility.

3.6. Determination of L-lactate in serum samples

To test the accuracy of the proposed method, the L-lactate biosensor was tested to determine the L-lactate concentration in human serum samples of three healthy volunteers. The real samples were diluted 1000 times with 0.1 M pH 7.4 PBS before performing ECL measurements. The standard addition method was followed, and the L-lactate concentration in real samples was determined from the calibration curve. The L-lactate concentrations in the serum samples were found to be 0.156, 0.232, and 0.183 mM, respectively. Control experiments were performed by using a spectrophotometric method at a local hospital. As shown in Table S1, the results obtained by our developed biosensor are in accordance with those tested by hospital, demonstrating that the presented biosensor can be used for monitoring L-lactate in human serum samples.

4. Conclusions

The $Ru(bpy)_3^{2+}$/POM@mrGO hybrid has been prepared by a facile approach for the fabrication of magneto-controlled ECL sensor. The coated POM films might perform versatile roles in the hybrid preparation and sensor performance: (1) protective layer of Fe_3O_4; (2) anchoring sites for the immobilization of Ru $(bpy)_3^{2+}$; and (3) electrocatalyst to the NADH oxidation. Benefit from the versatile POM film and the large surface area of mrGO, the magnetic field-driven modification of $Ru(bpy)_3^{2+}$/POM@mrGO hybrid showed stable and large response to NADH oxidation. On the basis of these findings, the surface-confined hybrid could be applied as a transduction platform for the ECL biosensor with LDH as a model dehydrogenase. The wide linear range and low detection limit for L-lactate declared its great potential applications in dehydrogenase-based ECL biosensors. This work provides a facile approach to immobilize ECL species within versatile POM@mrGO support matrix as well as promotes the development of magneto-controlled ECL biosensors directed to practical application in analytical and bio-analytical field.

Acknowledgments

The present work was supported by the National Natural Science Foundation of China (Nos. 21175061, 21375050, and 31271620), the Natural Science Foundation of Jiangsu province (No. BK20130481), China Postdoctoral Science Foundation (No. 2012M520998), Key Laboratory of Modern Agriculture Equipment and Technology (No. NZ201109), Jiangsu Planned Projects for Postdoctoral Research Funds (1301141C), and Research Foundation of Jiangsu University (12JDG087).

Appendix A. Supplementary material

Supplementary data associated with this article can be found in the online version at http://dx.doi.org/10.1016/j.bios.2014.02.005.

References

Ao, Y.H., Wang, P.F., Wang, C., Hou, J., Qian, J., 2013. Appl. Surf. Sci. 271, 265–270.
Ballesta–Claver, J., Valencia–Mirón, M.C., Capitán–Vallvey, L.F., 2008. Anal. Chim. Acta 629 (1–2), 136.
Bertoncello, P., Forster, R.J., 2009. Biosens. Bioelectron. 24 (11), 3191–3200.
Cao, H.M., Hu, X.Q., Hu, C.Y., Zhang, Y., Jia, N.Q., 2013. Biosens. Bioelectron. 41 (15), 911–915.
Chandra, V., Park, J., Chun, Y., Lee, J.W., Hwang, I.C., Kim, K.S., 2010. ACS Nano 4 (7), 3979–3986.
Cheng, J.J., Di, J.W., Hong, J.H., Yao, K.A., Sun, Y.B., Zhuang, J.Y., Xu, Q., Zhang, H.E., Bi, S.P., 2008. Talanta 76 (5), 1065–1069.
Choi, H.N., Yoon, S.H., Lyu, Y.K., Lee, W.Y., 2007. Electroanalysis 19 (4), 459–465.
Chovin, A., Garrigue, P., Sojic, N., 2006. Bioelectrochemistry 69 (1), 25–33.
Deng, L., Zhang, L.H., Shang, L., Guo, S.J., Wen, D., Wang, F.A., Dong, S.J., 2009. Biosens. Bioelectron. 24 (7), 2273–2276.
Du, Y., Wei, H., Kang, J., Yan, J., Yin, X.B., Yang, X., Wang, E., 2005. Anal. Chem. 77 (24), 7993–7997.
Fukuzumi, S., Inada, O., Suenobu, T., 2003. J. Am. Chem. Soc. 125 (16), 4808–4816.
Gao, W., Xia, X.h., Xu, J.J., Chen, H.Y., 2007. J. Phys. Chem. C 111 (33), 12213–12219.
Goran, J.M., Lyon, J.L., Stevenson, K.J., 2011. Anal. Chem. 83 (21), 8123–8129.
Haghighi, B., Bozorgzadeh, S., 2011. Talanta 85 (4), 2189–2193.
He, H.K., Gao, C., 2010. ACS Appl. Mater. Interfaces 2 (11), 3201–3210.
Hu, Y.W., Hua, S.C., Li, F.H., Jiang, Y.Y., Bai, X.X., Li, D., Niu, L., 2011. Biosens. Bioelectron. 26 (11), 4355–4361.
Jahan, M., Bao, Q.L., Loh, K.P., 2012. J. Am. Chem. Soc. 134 (15), 6707–6713.
Jin, Y.C., Qian, J., Wang, K., Yang, X.W., Dong, X.Y., Qiu, B.J., 2013. J. Electroanal. Chem. 693, 79–85.
Kim, D.J., Lyu, Y.K., Choi, H.N., Min, I.H., Lee, W.Y., 2005. Chem. Commun. 23, 2966–2968.
Li, M.J., Chen, Z.F., Yam, V.W.W., Zu, Y.B., 2008. ACS Nano 2 (5), 905–912.
Li, Y.B., Zhang, Z.J., Li, J.S., Li, H.G., Chen, Y., Liu, Z.H., 2011. Talanta 84 (3), 690–695.
Li, Y.L., Yang, X.R., Yang, F., Wang, Y.P., Zheng, P.H., Liu, X.X., 2012. Electrochim. Acta 66, 188–192.
Liao, N., Zhuo, Y., Chai, Y.Q., Xiang, Y., Han, J., Yuan, R., 2013. Biosens. Bioelectron. 45 (15), 189–194.
Liang, J.J., Huang, Y., Oh, J.Y., Kozlov, M., Sui, D., Fang, S.L., Baughman, R.H., Ma, Y.F., Chen, Y.S., 2011. Adv. Funct. Mater. 21 (19), 3778–3784.
Lin, Z.J., Chen, X.M., Jia, T.T., Wang, X.D., Xie, Z.X., Oyama, M., Chen, X., 2009. Anal. Chem. 81 (2), 830–833.
Liu, L.L., Bao, J.C., Fang, M., Li, L.F., Dai, Z.H., 2009. Sens. Actuators B: Chem. 139 (2), 527–531.
Mao, L., Yuan, R., Chai, Y.Q., Zhuo, Y., Yang, X., Yuan, S.R., 2010a. Talanta 80 (5), 1692–1697.
Mao, L., Yuan, R., Chai, Y.Q., Zhuo, Y., Yang, X., 2010b. Sens. Actuators B: Chem. 149 (1), 226–232.
Martínez, O.A., Ballesta, C.J., Palma, A.J., Valencia, Mirón, M.C., Capitán, V.L.F., 2009. Sensors 9 (10), 7694–7710.

Milutinovic, M., Sallard, S., Manojlovic, D., Mano, N., Sojic, N., 2011. Bioelectrochemistry 82 (1), 63–68.
Moretto, L.M., Kohls, T., Badocco, D., Pastore, P., Sojic, N., Ugo, P., 2010. J. Electroanal. Chem. 640 (1–2), 35–41.
Perez, S., Sanchez, S., Fabregas, E., 2012. Electroanalysis 24 (4), 967–974.
Qian, J., Zhou, Z.X., Cao, X.D., Liu, S.Q., 2010. Anal. Chim. Acta 665 (1), 32–38.
Qian, L., Yang, X.R., 2007. Adv. Funct. Mater. 17, 1353–1358.
Shimomura, T., Sumiya, T., Ono, M., Ito, T., Hanaoka, T., 2012. Anal. Chim. Acta 714, 114–120.
Su, J., Cao, M.H., Ren, L., Hu, C.W., 2011. J. Phys. Chem. C 115 (30), 14469–14477.
Sun, X.P., Du, Y., Dong, S.J., Wang, E.K., 2005. Anal. Chem. 77 (24), 8166–8169.
Sun, X.P., Du, Y., Zhang, L.X., Dong, S.J., Wang, E.K., 2007. Anal. Chem. 79 (6), 2588–2592.
Teymourian, H., Salimi, A., Hallaj, R., 2012. Biosens. Bioelectron. 33 (1), 60–68.
Wang, K., Li, H.N., Ju, C., Luo, Z.J., Dai, L.N., Li, H.M., 2010. Talanta 82 (3), 1068–1071.
Wang, K., Liu, Q., Guan, Q.M., Wu, J., Li, H.N., Yan, J.J., 2011. Biosens. Bioelectron. 26 (5), 2252–2257.
Wu, J.W., Mei, W.J., Chen, X.P., Liu, J.C., Li, H., 2013. Electrochim. Acta 103, 1–8.
Xu, Y.H., Lv, Z.Z., Xia, Y., Han, Y.C., Lou, B.H., Wang, E.K., 2013. Anal. Bioanal. Chem. 405, 3549–3558.
Yang, X., Yuan, R., Chai, Y.Q., Zhuo, Y., Mao, L., Yuan, S.R., 2010. Biosens. Bioelectron. 25 (7), 1851–1855.
Zhan, W., Bard, A.J., 2007. Anal. Chem. 79 (2), 459–463.
Zhang, L.H., Xu, Z.A., Dong, S.J., 2006. Anal. Chim. Acta 575 (1), 52–56.
Zhang, L.H., Liu, B.F., Dong, S.J., 2007. J. Phys. Chem. B 111 (35), 10448–10452.
Zhang, B., Shi, S.X., Shi, W.Y., Sun, Z.Y., Kong, X.G., Wei, M., Duan, X., 2012. Electrochim. Acta 67, 133–139.